

A LARGE, UNIFORM SAMPLE OF X-RAY-EMITTING ACTIVE GALACTIC NUCLEI FROM THE *ROSAT* ALL SKY AND SLOAN DIGITAL SKY SURVEYS: THE DATA RELEASE 5 SAMPLE

SCOTT F. ANDERSON,<sup>1</sup> BRUCE MARGON,<sup>2</sup> WOLFGANG VOGES,<sup>3</sup> RICHARD M. PLOTKIN,<sup>1</sup> DAVID SYPHERS,<sup>1</sup> DARYL HAGGARD,<sup>1</sup>  
 MATTHEW J. COLLINGE,<sup>4</sup> JILLIAN MEYER,<sup>1</sup> MICHAEL A. STRAUSS,<sup>4</sup> MARCEL A. AGÜEROS,<sup>1</sup> PATRICK B. HALL,<sup>5</sup>  
 L. HOMER,<sup>1</sup> ŽELJKO IVEZIĆ,<sup>1</sup> GORDON T. RICHARDS,<sup>6</sup> MICHAEL W. RICHMOND,<sup>7</sup> DONALD P. SCHNEIDER,<sup>8</sup>  
 GREGORY STINSON,<sup>1</sup> DANIEL E. VANDEN BERK,<sup>8</sup> AND DONALD G. YORK<sup>9</sup>

Received 2006 July 24; accepted 2006 September 12

## ABSTRACT

We describe further results of a program aimed at yielding  $\sim 10^4$  fully characterized optical identifications of *ROSAT* X-ray sources. Our program employs X-ray data from the *ROSAT* All Sky Survey (RASS) and both optical imaging and spectroscopic data from the Sloan Digital Sky Survey (SDSS). RASS/SDSS data from 5740 deg<sup>2</sup> of sky spectroscopically covered in SDSS Data Release 5 provide an expanded catalog of 7000 confirmed quasars and other active galactic nuclei (AGNs) that are probable RASS identifications. Again, in our expanded catalog the identifications as X-ray sources are statistically secure, with only a few percent of the SDSS AGNs likely to be randomly superposed on unrelated RASS X-ray sources. Most identifications continue to be quasars and Seyfert 1 galaxies with  $15 < m < 21$  and  $0.01 < z < 4$ , but the total sample size has grown to include very substantial numbers of even quite rare AGNs, e.g., it now includes several hundreds of candidate X-ray-emitting BL Lac objects and narrow-line Seyfert 1 galaxies. In addition to exploring rare subpopulations, such a large total sample may be useful when considering correlations between the X-ray and the optical and may also serve as a resource list from which to select the “best” object (e.g., X-ray-brightest AGN of a certain subclass at a preferred redshift or luminosity) for follow-up X-ray spectral or alternate detailed studies.

**Key words:** catalogs — quasars: general — surveys — X-rays

**Online material:** machine-readable tables

## 1. INTRODUCTION

The premier X-ray-imaging survey of the astronomical sky is the *ROSAT* All Sky Survey (RASS; Voges et al. 1999, 2000). In the 1990s, RASS surveyed most of the celestial sphere in the 0.1–2.4 keV range with the Position Sensitive Proportional Counter (PSPC; Pfeffermann et al. 1987) to a typical limiting sensitivity of  $\sim 10^{-13}$  ergs cm<sup>-2</sup> s<sup>-1</sup>, cataloging more than  $10^5$  X-ray sources in the RASS Bright and Faint Source Catalogs.

With RASS’s typical X-ray positional uncertainty of order  $\sim 10''$ – $30''$ , the effort involved in optically identifying a large fraction of the cataloged abundant RASS sources may appear daunting; and yet, several large-scale identification efforts are currently making substantial progress. Thousands of optical identifications for RASS sources are now suggested, albeit with various levels of identification confidence on the nature of the counterparts, ranging from statistical cross-correlations with Schmidt photographic plate images (e.g., see radio/optical/X-ray matches cataloged in Flesch & Hardcastle 2004), to op-

tical spectral identification estimates from low spectral resolution photographic Schmidt objective prism plates (see, e.g., Zickgraf et al. 2003; Mickaelian et al. 2006), to digital optical photometry and multiobject spectrophotometry (see, e.g., RASS Bright and Faint Source Catalog identifications in Anderson et al. 2003).

For comparison to such recent RASS efforts involving thousands of suggested optical identifications each, it may be recalled that the most complete optical identification effort at similar depth from *Einstein* X-ray data was the Extended Medium Sensitivity Survey (EMSS; see, e.g., Gioia et al. 1984; Stocke et al. 1991). Quasars/active galactic nuclei (AGNs) were the predominant class in the EMSS, accounting for about half of the  $\sim 800$  *Einstein* identifications. Although the EMSS total of  $\sim 400$  AGN identifications is quite large in aggregate, certain subsets are critically small when subdivided; for example, although the EMSS provided fundamental insights into BL Lac object evolution (Morris et al. 1991), the entire EMSS sample included only  $\sim 40$  BL Lac objects.

In order to substantively expand on such earlier *Einstein* programs, current efforts should provide samples significantly exceeding  $\sim 10^3$  spectroscopically secure optical identifications. Our approach, detailed previously in Anderson et al. 2003 (hereafter Paper I), relies on the very good sensitivity match between AGNs detectable in X-rays with RASS and AGNs accessible to good-quality optical spectra with the Sloan Digital Sky Survey (SDSS; York et al. 2000). Our ultimate aim has been the cataloging and characterization of  $\sim 10^4$  X-ray identifications; the AGNs in this sample are not only statistically secure in their identifications as X-ray sources but are also accompanied by high-quality and uniform data in the X-ray from RASS and in the optical (both photometry and spectroscopy) from SDSS.

<sup>1</sup> Department of Astronomy, University of Washington, Seattle, WA, USA; anderson@astro.washington.edu, plotkin@astro.washington.edu.

<sup>2</sup> Space Science Telescope Institute, Baltimore, MD, USA; margon@stsci.edu.

<sup>3</sup> Max-Planck-Institute für extraterrestrische Physik, Garching, Germany; wvoges@mpe.mpg.de.

<sup>4</sup> Princeton University Observatory, Princeton, NJ, USA.

<sup>5</sup> Department of Physics and Astronomy, York University, Toronto, ON, Canada.

<sup>6</sup> Department of Physics and Astronomy, The Johns Hopkins University, Baltimore, MD, USA.

<sup>7</sup> Department of Physics, Rochester Institute of Technology, Rochester, NY, USA.

<sup>8</sup> Department of Astronomy and Astrophysics, The Pennsylvania State University, University Park, PA, USA.

<sup>9</sup> Astronomy and Astrophysics Center, University of Chicago, Chicago, IL, USA.

In § 2 we briefly review relevant aspects of the SDSS data and the selection and confirmation of candidate AGN optical counterparts from SDSS; detailed descriptions of these aspects and a much more complete set of references can be found in Paper I. In § 3 we present results from our RASS/SDSS program for 5740 deg<sup>2</sup> of sky (about 4 times the area coverage considered in Paper I), providing an updated and expanded catalog of X-ray and optical properties of 7000 likely SDSS AGN identifications for RASS X-ray sources. In §§ 3 and 4 we discuss some AGN subclasses of special interest, including more than 260 X-ray-emitting BL Lac candidates and 770 candidate X-ray-emitting narrow-line Seyfert 1 galaxies (NLS1s) and related quasars. Section 5 discusses the reliability of the identifications and some ensemble properties of the expanded sample. Section 6 provides an updated example optical/X-ray correlation study. A short summary is provided in § 7.

## 2. SELECTED ASPECTS OF SDSS RELEVANT TO RASS IDENTIFICATIONS

The SDSS is creating an optical digital imaging and spectroscopic database of a large portion of the celestial sphere, primarily in a region approaching  $\sim 10^4$  deg<sup>2</sup> centered on the north Galactic polar cap. The optical data are obtained by a dedicated 2.5 m telescope located at Apache Point Observatory, New Mexico, equipped with a large-format mosaic camera that can image  $\sim 10^2$  deg<sup>2</sup> in five colors ( $u, g, r, i, z$ ) in a single night, as well as a multifiber spectrograph that obtains the spectra of 640 objects within a 7 deg<sup>2</sup> field simultaneously. The imaging database is used to select objects for the SDSS spectroscopic survey, which includes ( $\lambda/\Delta\lambda \sim 1800$ ) spectrophotometry covering a broad (3800–9200 Å) wavelength range for  $10^6$  galaxies,  $10^5$  quasars, and  $10^5$  stars. Details on SDSS hardware, software, and astrometric, photometric, and spectral data can be found in a variety of papers, including Fukugita et al. (1996), Gunn et al. (1998), Lupton et al. (1999), York et al. (2000), Hogg et al. (2001), Stoughton et al. (2002), Smith et al. (2002), Pier et al. (2003), Ivezić et al. (2004), Gunn et al. (2006), and Tucker et al. (2006). A description of the previous SDSS Public Data Release (DR4) is given by Adelman-McCarthy et al. (2006).

The depths of RASS and SDSS are well matched. For example, quasars and BL Lac objects are known to have extreme X-ray-to-optical flux ratios of order  $\log(f_X/f_{\text{opt}}) \sim 1.0$ –1.5 (Stocke et al. 1991), so even unusually faint RASS optical counterparts will have magnitudes brighter than  $m < 20$ –21. The SDSS imaging survey at this depth provides accurate colors and magnitudes for nearly all RASS counterparts, and SDSS multiobject follow-up spectroscopy also typically yields excellent quality data. The RASS/SDSS area is also covered by the NRAO VLA Sky Survey and/or FIRST (Faint Images of the Radio Sky at Twenty cm) 20 cm radio surveys (Condon et al. 1998; Becker et al. 1995), providing radio information for nearly all RASS/SDSS objects.

A detailed description of the SDSS “target selection pipeline” (Stoughton et al. 2002) algorithms applicable to RASS sources is provided in Paper I, so here we provide an abbreviated summary. Optical objects in the SDSS photometric catalogs are automatically cross-correlated with X-ray sources in the RASS Bright and Faint Source catalogs, and those SDSS optical objects within 1' of the X-ray-source positions are initially flagged as potential positional matches to be considered further. Due to limitations on the number of spare SDSS fibers available for *ROSAT* identifications and a 55'' restriction on the minimum separation of adjacent fibers, we especially favor confirming optical spectroscopy of a single, high-priority SDSS candidate counterpart within

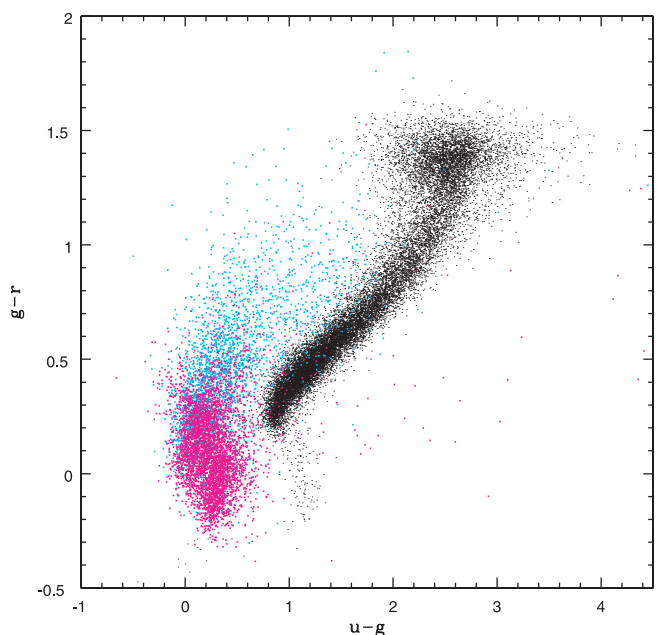


FIG. 1.— Optical SDSS colors of 7000 spectroscopically confirmed quasars and other X-ray-emitting AGNs in our updated sample overplotted for comparison on the locus of 10,000 anonymous SDSS stellar objects (*black dots*). The magenta dots show the SDSS colors of quasi-stellar X-ray identifications that are unresolved in SDSS images, while cyan dots show the colors of AGNs morphologically resolved in the SDSS. Note the good color separation of the large majority of the confirmed quasar/AGN identifications.

27.5'' of the RASS X-ray position for each of the  $\sim 10^4$  highest significance RASS sources (X-ray detection likelihood  $\geq 10$ ) that lie within the joint RASS/SDSS sky coverage. SDSS spectroscopic limits for RASS candidate counterparts are approximately in the range  $15 < m < 20.5$ , where  $m$  refers here to the  $g, r, \text{ or } i$  passbands.

Each SDSS optical object imaged in a RASS error circle is assigned to a graded (A, B, C, D, or E) priority bin for follow-up SDSS optical spectroscopy. The priority bins are based on the typical ratios of X-ray to optical flux for known subclasses of X-ray emitters, with SDSS optical magnitudes, colors, and image morphology, as well as FIRST radio data, serving as indicators of the likely object class during spectroscopic target selection. The “ROSAT\_A” and “ROSAT\_B” (two highest priority) categories are specifically aimed at AGNs and encompass about 92% of the identifications presented here. These two categories are also highly efficient, with 85% of all targeted ROSAT\_A and ROSAT\_B objects returning spectra of AGNs. ROSAT\_A objects are triple positional coincidences of a RASS X-ray source, an SDSS optical object, and a FIRST radio source, especially aimed at BL Lac objects (and other X-ray/radio-emitting quasars). ROSAT\_B is assigned to SDSS objects having unusual optical colors indicative of AGNs/quasars (Richards et al. 2002); UV excess and more sophisticated multicolor approaches are consulted, e.g., see Figure 1. The reader is referred to Paper I for details on the other *ROSAT* target selection categories.

In addition, SDSS objects that are part of the main optical spectroscopic surveys of  $10^6$  galaxies and  $10^5$  quasars are assigned their spectroscopic fibers first, even before the SDSS/RASS target selection algorithms (making use of spare fibers) come into play. As a bonus to this identification program, SDSS spectra are thus available for the vast majority of such “tiled targets” (Blanton et al. 2003) falling fortuitously in RASS error circles; these include most galaxies to Petrosian  $r < 17.77$ , SDSS

objects to  $i < 19.1$  with quasar colors, and FIRST radio sources with optical point-spread function (PSF) morphology to  $i < 19.1$ . On the other hand, a galaxy targeted as part of the SDSS galaxy redshift survey sample and merely falling by chance near a RASS error circle may sometimes eliminate a desired *ROSAT* target from any chance of receiving a spectroscopic fiber.

Thus, our expanded RASS/SDSS catalog is not a “complete” sample, although in practice we expect that the catalog may eventually prove to be reasonably complete for most classes of X-ray-emitting quasars and AGNs with  $15 < m < 19$ . For these objects quasar target selection completeness is confirmed to be high (Vanden Berk et al. 2005), and these may be selected for SDSS spectra by either sparse-fiber *ROSAT* or tiled-fiber quasar target selection categories.

### 3. EXPANDED CATALOG OF 7000 X-RAY-EMITTING AGNs FROM RASS/SDSS

The expanded catalog of RASS/SDSS identifications is presented in this section. The emphasis in this installment of the RASS/SDSS catalog is on a set of 7000 X-ray-emitting quasars/AGNs. About 1200 of these constituted our original installment of the RASS/SDSS AGNs catalog presented in Paper I. For the full sample of 7000 AGNs, the identifications are statistically secure, as discussed in § 5.

We have examined an early version of the Data Release 5 (DR5) database and identified 15,129 SDSS spectra that fall within  $1'$  of a RASS source. All of these spectra have been examined by a variety of methods, both algorithmic and visual, to search for plausible AGN identifications for the corresponding RASS X-ray sources. Our examination of the SDSS spectra taken within RASS error circles emphasizes searching especially for the following sets of AGNs: (1) classic AGNs/quasars with strong, broad emission lines; (2) AGNs with narrower line components; and (3) BL Lac objects with weak or absent spectral features.

#### 3.1. Quasars and Other AGNs with Strong, Broad Permitted Lines

In Tables 1 and 2 we present an updated catalog of spectroscopically confirmed RASS/SDSS quasars and closely related AGNs having strong, broad permitted emission lines. All are in SDSS DR5 and have optical positions within  $1'$  of RASS X-ray sources. We present the entire updated RASS/SDSS AGN catalog, including both new objects and those presented previously in Paper I (or elsewhere in the literature). Paper I included optical data from very early on in the SDSS program (e.g., extending back to the “Early Data Release” before SDSS photometric calibrations were complete; Stoughton et al. 2002), so here we catalog all counterparts with their uniform SDSS DR5 photometric and spectroscopic parameters.

Included under the category of “broad-line” quasars are RASS/SDSS objects whose spectra show the characteristic strong optical emission lines of AGNs, with broad permitted emission having a velocity width in excess of  $1000 \text{ km s}^{-1}$  FWHM; the latter value is also that used in the DR3 quasar catalog of Schneider et al. (2005) and is close to the value of  $1200 \text{ km s}^{-1}$  that separates a bimodal line-width distribution seen in SDSS Seyfert galaxies (Hao et al. 2005). In order to identify such broad-lined quasars we first considered those spectra in which the SDSS spectroscopic 1D pipeline software (Stoughton et al. 2002) returned a best-fit Gaussian FWHM exceeding  $1000 \text{ km s}^{-1}$  for any of the following emission lines: Ly $\alpha$ , N v  $\lambda 1240$ , Si iv  $\lambda 1400$  (blend), C iv  $\lambda 1549$ , C iii]  $\lambda 1909$ , Mg ii  $\lambda 2800$ , H $\gamma$ , H $\beta$ , or H $\alpha$ . Of the 15,129 SDSS DR5 spectra taken in RASS error circles,

7220 spectra appeared to satisfy this initial pipeline-based emission-line-width criteria within the DR5 database. An additional 17 spectra were found in a subsequent by-eye examination (discussed in § 3.2) that are also clearly predominantly broad-lined AGNs but which failed the algorithmic cut discussed above based on spectroscopic pipeline measures; for example, this group includes some broad absorption line QSOs (BALQSOs) and some cases with spectral reduction problems.

We visually reexamined all 7237 spectra to confirm their nature, as well as to verify the pipeline redshifts. Among these, 6582 were visually confirmed to indeed be spectra of broad-line quasars, with only 9 requiring significant redshift corrections to the pipeline estimates. From the surviving list of 6582 confirmed broad-line AGN spectra, there are 6224 distinct objects; that is, about 5% of these AGNs have more than one SDSS spectrum available in DR5. Although the line-width selection in this paper is based almost entirely on SDSS pipeline Gaussian-fit measures, 99% of the AGNs cataloged in Paper I (where classifications were based on manual line measures) are also recovered in this paper; the substantial recovery fraction is not a surprise, of course, but worthy of verification given our far heavier reliance in the current paper on SDSS pipeline spectroscopic measures. Note also that we avoid any luminosity cuts, and so Tables 1 and 2 include not just most classic quasars and Seyfert 1 galaxies but also many Seyfert 1.5–1.9 galaxies and even many rare objects such as NLS1s.

All AGNs have confirming, high-quality SDSS optical spectra and imaging, uniformly reduced as part of DR5. See Figure 2 for representative examples of their SDSS spectra.

Following our format in Paper I, Table 1 includes mainly empirical characteristics of the 6224 X-ray-emitting RASS/SDSS broad-line quasar/AGN counterparts, while Table 2 provides mainly derived information. Table 1 is ordered according to the right ascension (J2000.0) of the RASS X-ray source: Column (1) lists the X-ray position, using right ascension and declination nomenclature. Column (2) provides the optical position/nomenclature (J2000.0) of the suggested SDSS quasar/AGN counterpart. Columns (3)–(7) provide uniform DR5 optical PSF photometry in the five SDSS passbands (e.g., Fukugita et al. 1996) in the asinh AB system (Lupton et al. 1999). Column (8) provides the value of the SDSS imaging morphology parameter: type 6 indicates a stellar/unresolved optical morphology, while type 3 indicates an extended/resolved (i.e., galaxy) morphology. Column (9) provides the redshift measured from SDSS spectra. The remaining columns of Table 1 emphasize empirical X-ray data from the RASS catalogs (see, e.g., Voges et al. 1999, 2000). Column (10) provides the RASS X-ray-source count rate (counts  $\text{s}^{-1}$ ) in the 0.1–2.4 keV broad band, corrected for vignetting. Column (11) gives the RASS exposure time in seconds. Columns (12) and (13) provide X-ray hardness ratios. Column (14) gives the X-ray-source detection likelihood. Column (15) gives the observed X-ray flux in the 0.1–2.4 keV band; we used the PIMMS software to convert RASS count rates into X-ray fluxes, assuming a power-law X-ray spectrum with energy index  $\alpha_X = 1.5$ , typical of low-redshift quasars in the RASS PSPC bandpass (see, e.g., Schartel et al. 1996).

In Table 2 we present further catalog information on the 6224 broad-line RASS/SDSS AGNs, emphasizing derived quantities. For cross reference to Table 1, we repeat in columns (1) and (2) the RASS X-ray source and optical counterpart name/position, respectively. Column (3) provides the  $g$ -band PSF magnitude, but here extinction-corrected according to the reddening maps of Schlegel et al. (1998). Column (4) repeats the SDSS spectroscopic redshift. Column (5) gives the X-ray flux (units of

TABLE 1  
OBSERVED PARAMETERS OF BROAD-LINE RASS/SDSS AGNs

RASS X-Ray Source RXS J (1)	SDSS Optical Counterpart SDSS J (2)	<i>u</i> (3)	<i>g</i> (4)	<i>r</i> (5)	<i>i</i> (6)	<i>z</i> (7)	Opt. Morphology (8)	Redshift (9)	X-Ray Count Rate (10)	Exp. Time (11)	HR1 (12)	HR2 (13)	Det. Likelihood (14)	$f_X \times 10^{13}$ (15)
000011.9+000223 .....	000011.96+000225.3	18.24	17.97	18.02	17.96	17.91	6	0.479	0.0219	364	−0.01	−1.00	9	2.20
000024.1+152026 .....	000024.02+152005.4	19.41	19.18	18.99	19.08	19.13	6	0.989	0.0133	463	−0.05	−1.00	8	1.41
000100.8−102318 .....	000102.18−102326.9	18.98	18.69	18.33	18.24	17.66	6	0.294	0.0284	340	0.37	−0.13	8	2.76
000117.2+141150 .....	000116.00+141123.0	19.01	18.68	18.70	18.56	18.16	6	0.404	0.0155	405	1.00	0.14	8	1.74
000133.1+145601 .....	000132.83+145608.0	19.22	19.20	19.25	19.04	18.39	3	0.399	0.0388	473	0.18	−0.86	21	4.28

NOTES.—Table 1 is published in its entirety in the electronic edition of the *Astronomical Journal*. A portion is shown here for guidance regarding its form and content.

TABLE 2  
DERIVED PARAMETERS OF BROAD-LINE RASS/SDSS AGNs

RASS X-Ray Source RXS J (1)	SDSS Optical Counterpart SDSS J (2)	$g_o$ (3)	Redshift (4)	$f_X^c \times 10^{13}$ (5)	$\log(L_X)$ (6)	$\log(l_{opt})$ 2500 Å (7)	$\log(l_X)$ 2 keV (8)	$\alpha_{ox}$ (9)	Comment (10)
000011.9+000223 .....	000011.96+000225.3	17.85	0.479	5.42	44.76	30.14	26.22	1.50	LBQS 2357–0014
000024.1+152026 .....	000024.02+152005.4	19.02	0.989	3.60	45.41	30.37	26.88	1.34	...
000100.8–102318 .....	000102.18–102326.9	18.53	0.294	6.60	44.32	29.40	25.78	1.39	...
000117.2+141150 .....	000116.00+141123.0	18.46	0.404	4.68	44.51	29.73	25.97	1.44	...
000133.1+145601 .....	000132.83+145608.0	19.03	0.399	11.36	44.88	29.49	26.34	1.21	...

NOTES.—Table 2 is published in its entirety in the electronic edition of the *Astronomical Journal*. A portion is shown here for guidance regarding its form and content.

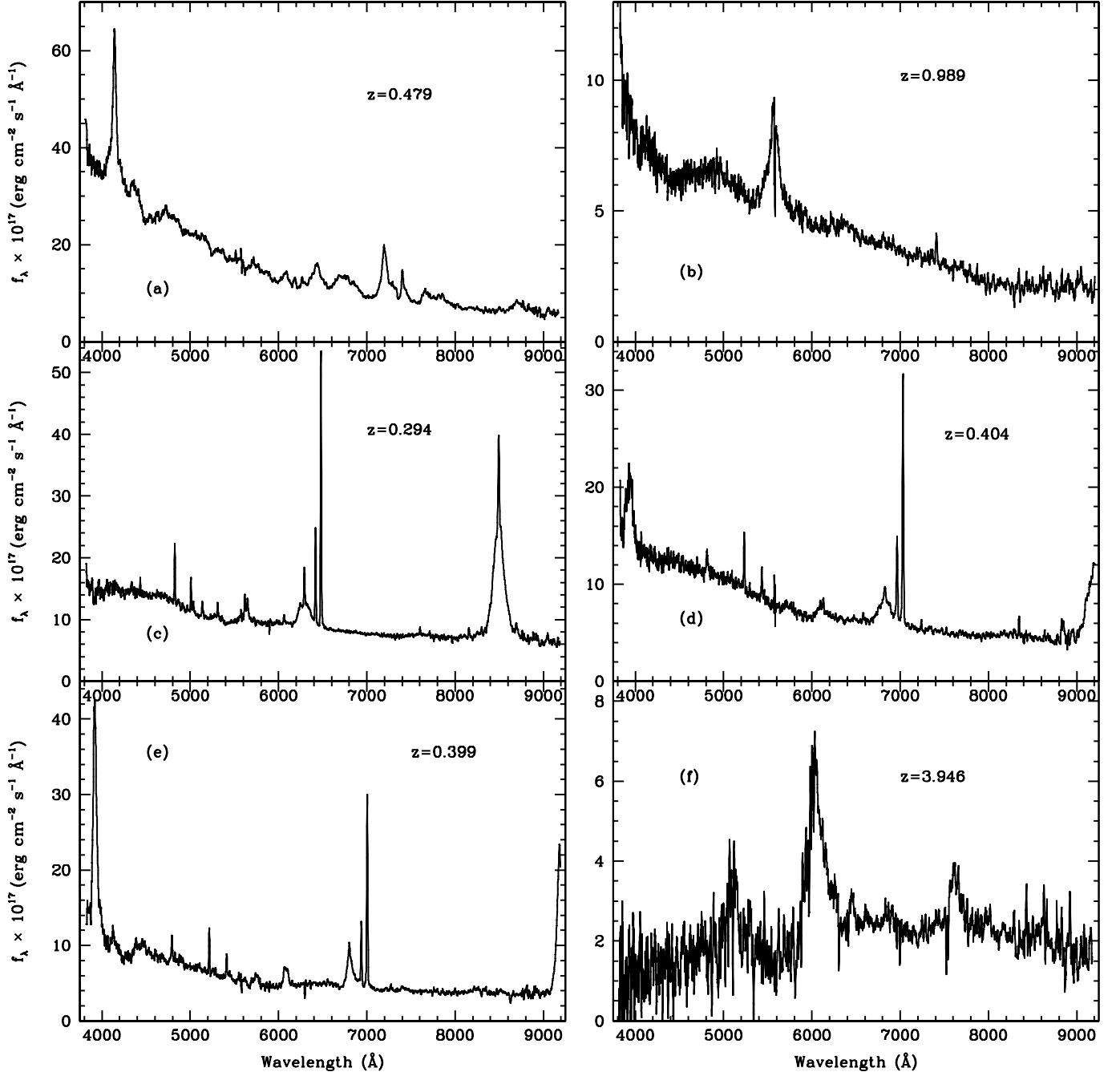


FIG. 2.—Representative SDSS optical spectra for RASS/SDSS X-ray-emitting quasars/AGNs with broad permitted emission lines, as discussed in § 3.1. Shown (a–e) are spectra smoothed with a seven-point boxcar for the first five objects listed in Tables 1 and 2, along with (f) a high-redshift case reflecting the very broad range of redshifts sampled. All 6224 broad-line AGNs cataloged have similar high-quality SDSS spectroscopy. (a) SDSS J000011.96+000225.3. (b) SDSS J000024.02+152005.4. (c) SDSS J000102.18–102326.9. (d) SDSS J000116.00+141123.0. (e) SDSS J000132.83+145608.0. (f) SDSS J081009.95+384757.0.

$10^{-13}$  ergs  $\text{s}^{-1} \text{cm}^{-2}$ ) in the 0.1–2.4 keV band, now corrected for absorption within the Galaxy, with X-ray-absorbing columns estimated using the  $N_{\text{H}}$  column-density measures of the Stark et al. (1992) 21 cm maps. Columns (6), (7), and (8) give the logarithms of inferred broadband (0.1–2.4 keV) X-ray luminosity (units of ergs  $\text{s}^{-1}$ ), UV/optical monochromatic luminosity (cgs units of ergs  $\text{s}^{-1} \text{Hz}^{-1}$ ) at a frequency corresponding to rest frame 2500 Å, and monochromatic X-ray luminosity (cgs) at 2 keV; we adopt values of  $H_0 = 70 \text{ km s}^{-1} \text{Mpc}^{-1}$ ,  $\Omega_M = 0.3$ , and  $\Omega_\Lambda = 0.7$  for deriving the luminosities in Table 2. In converting from corrected broadband (X-ray 0.1–2.4 keV and optical  $g$ -band) fluxes to luminosities, we again assume an X-ray power-law spectrum with energy index  $\alpha_X = 1.5$  and an optical power law with energy index  $\alpha_o = 0.5$ . Column (9) lists  $\alpha_{\text{ox}}$ , the slope of a hypothetical power law in energy from the UV/optical to X-ray (i.e., connecting 2500 Å and 2 keV). Column (10) provides brief comments, for example, noting selected objects that are radio sources, listing an alternate name (shortened, if needed, to the first 20 characters) taken from NASA/IPAC Extragalactic Database for about 10% of the quasars, and noting the  $\sim 1.5\%$  of the cases for which two of our cataloged AGNs fall within the same RASS error circle (the latter are denoted by “ambigID” in the comments, and eight such cases involve AGN pairs at similar redshifts).

### 3.2. X-Ray-emitting AGNs Having Narrower Permitted Emission Lines

We have also examined the remainder of the 15,129 spectra of SDSS objects in RASS error circles, as some bona fide AGN identifications will fail to satisfy the broad-line (based on a simple single-component Gaussian pipeline fit) criterion discussed in the previous section. Our experience from Paper I verified that examining all relevant spectra helps ensure fuller inclusion of such X-ray-emitting AGN subclasses as NLS1s (see § 4.1 for NLS1 details) and Seyfert 1.5, 1.8, and 1.9 galaxies; i.e., objects with broad-line regions related to those of classic quasars and Seyfert 1 galaxies but that may be observed to have “narrower” ( $< 1000 \text{ km s}^{-1}$ ) permitted-line components as well. The catalog of “narrow-line” AGNs presented in this section is also extended to include Seyfert 2 and type 2 quasar candidates, whose optical spectra are even more strongly dominated by narrow emission lines. The additional narrow-line AGNs cataloged in this section are mainly from the lower redshift regime of our sample.

Following Paper I, for classification among this narrower lined group as Seyfert 1.5–1.8 galaxies, we manually verify from each SDSS spectrum that the full width near the continuum level (FWZI) of the  $\text{H}\beta$  emission line exceeds  $2500 \text{ km s}^{-1}$ , also verifying that the width of the  $\text{H}\beta$  line exceeds that of the  $[\text{O III}] \lambda 5007$  emission in the same object by at least  $\sim 1000 \text{ km s}^{-1}$ . Hence each such object has some “broad-line” component substantially wider than is typical of its narrow-line region.

We also select among the narrow-line group AGNs whose SDSS optical spectra lack strong, broad  $\text{H}\beta$  emission but that nonetheless do have a markedly broad (at least at the continuum level)  $\text{H}\alpha$  emission component. As in Paper I, we again refer to these objects loosely as Seyfert 1.9 galaxies, although many may be Seyfert 1.5–1.8 galaxies, where the signal-to-noise ratio (S/N) is merely low near  $\text{H}\beta$ . As in Paper I, we again very conservatively limit our Seyfert 1.9 candidate list to include just those cases with very broad  $\text{H}\alpha$ , requiring  $\text{FWZI}(\text{H}\alpha) > 6000 \text{ km s}^{-1}$ . (Note that many Seyfert 1.9 galaxies were properly identified by the DR5 pipeline as broad-lined AGNs based on the FWHM of  $\text{H}\alpha$  and so are already cataloged in the current paper under the broad-line criteria in § 3.1.)

Our narrow-line catalog also includes candidate X-ray-emitting Seyfert 2 galaxies and related AGNs. We reemphasize the warning of Paper I that historically a number of such possible cases found in earlier X-ray surveys have, when subsequently scrutinized with improved optical spectroscopy, ultimately been reclassified (e.g., Halpern et al. 1999) into one of the categories already considered above, e.g., NLS1, Seyfert 1.8, or Seyfert 1.9. However, inclusion of these X-ray-emitting Seyfert 2 candidates may, at the very least, call attention to especially subtle cases of X-ray-emitting Seyfert 1.8–1.9 galaxies or NLS1s that we otherwise might have missed. For most Seyfert 2 candidates we again adopt the criteria of Kewley et al. (2001) based on the relative line strengths of  $[\text{O III}] \lambda 5007/\text{H}\beta$ ,  $[\text{N II}] \lambda 6583/\text{H}\alpha$ , and  $[\text{S II}] \lambda 6717, 6731/\text{H}\alpha$ ; these line ratios define regions in “BPT diagrams” (Baldwin et al. 1981) populated by AGNs versus starbursts. For a few objects, especially those at  $z > 0.5$  where  $\text{H}\alpha$ ,  $[\text{N II}]$ , and/or  $[\text{S II}]$  measures are not available, we require only that  $[\text{O III}] \lambda 5007/\text{H}\beta > 3$ . Note that we use the SDSS pipeline Gaussian line-flux measures in this application. Tables 3 and 4 catalog empirical and derived information, respectively, for the additional 515 X-ray-emitting narrower lined AGNs discussed in this section; 405 of these have some observed broad-line component (e.g., NLS1s and Seyfert 1.5–1.9 galaxies), and an additional 110 are Seyfert 2 or type 2 quasar candidates. The comment column in Table 4 may include the spectral subclass type; these taxonomical classifications are tabulated to clarify why these narrower line AGNs did not satisfy the broad-line criteria discussed in § 3.1. Figure 3 shows selected SDSS spectra from this group of identifications, reflecting some of the diversity among these narrower lined X-ray-emitting AGNs.

### 3.3. BL Lac Candidates

We have also expanded our RASS/SDSS sample of BL Lac candidates to SDSS DR5. In Paper I we provided a list of 45 X-ray-emitting BL Lac objects and candidates, and additional cases from SDSS were presented as a subset of the more general spectroscopically selected SDSS optical BL Lac sample discussed in Collinge et al. (2005). The rarity of BL Lac objects demands large areal sky coverage such as that achievable from SDSS, and their unusual spectral energy distributions (with a lack of strong spectral features) generally allows efficient selection only via multiwavelength approaches—especially in radio, optical, and X-ray surveys (e.g., Stocke et al. 1991; Perlman et al. 1996; Laurent-Muehleisen et al. 1997; Bade et al. 1998a; see also a review by Urry & Padovani 1995).

We employ similar approaches within our ROSAT\_A target selection algorithm (as discussed in § 2) to obtain the updated DR5 sample of RASS/SDSS BL Lac candidates discussed here. We find (or recover) 181 objects we consider as *probable* X-ray-emitting RASS/SDSS BL Lac objects. For these higher confidence cases (1) the SDSS optical object is within  $1'$  of a RASS source; (2) the SDSS object is also a positional match to a radio source (conservatively taken as  $< 2''$  for matches to FIRST sources, or  $< 7''$  for matches to other radio catalogs); (3) our measures from the SDSS optical spectrum reveal no strong emission ( $\text{EW} < 5 \text{ Å}$ ); and (4) either there is no Ca II H and K break/depression evident in the SDSS optical spectrum or, if present, any such break must be weak. Following Stocke et al. (1991), we require the Ca II H and K break to have  $C \leq 0.25$ , where  $C = 0.14 + 0.86(f_{\lambda,+} - f_{\lambda,-})/f_{\lambda,+}$  and where  $f_{\lambda,-}$  and  $f_{\lambda,+}$  are the average specific fluxes over the wavelength ranges 3750–3950 and 4050–4250 Å, respectively (see, e.g., Landt et al. 2002; Dressler & Schectman 1987). We also find as *possible* BL Lac candidates

TABLE 3  
OBSERVED PARAMETERS OF RASS/SDSS AGNs HAVING NARROWER PERMITTED EMISSION

RASS X-Ray Source RXS J (1)	SDSS Optical Counterpart SDSS J (2)	<i>u</i> (3)	<i>g</i> (24)	<i>r</i> (5)	<i>i</i> (6)	<i>z</i> (7)	Opt. Morphology (8)	Redshift (9)	X-Ray Count Rate (10)	Exp. Time (11)	HR1 (12)	HR2 (13)	Det. Likelihood (14)	$f_X \times 10^{13}$ (15)
000202.5–103030 .....	000202.95–103038.0	18.06	17.59	17.25	16.81	16.63	3	0.103	0.0610	324	–0.12	–0.14	31	5.94
000250.8+000824 .....	000251.60+000800.7	20.54	19.48	18.67	18.21	17.88	3	0.107	0.0410	388	–0.32	0.09	9	4.10
001056.7–090100 .....	001056.25–090109.9	19.14	18.06	17.57	17.10	16.90	3	0.081	0.0283	343	0.49	1.00	10	2.82
001618.5+011528 .....	001617.83+011522.0	21.06	19.67	18.69	18.18	17.88	3	0.217	0.0398	402	–0.13	–0.14	18	3.78
002608.2–000544 .....	002608.38–000547.0	20.73	19.57	18.81	18.32	17.93	3	0.107	0.0228	415	0.81	0.49	13	2.11

NOTES.—Table 3 is published in its entirety in the electronic edition of the *Astronomical Journal*. A portion is shown here for guidance regarding its form and content.

TABLE 4  
DERIVED PARAMETERS OF RASS/SDSS AGNs HAVING NARROWER PERMITTED EMISSION

RASS X-Ray Source RXS J (1)	SDSS Optical Counterpart SDSS J (2)	$g_o$ (3)	Redshift (4)	$f_X^c \times 10^{13}$ (5)	$\log(L_X)$ (6)	$\log(l_{opt})$ 2500 Å (7)	$\log(l_X)$ 2 keV (8)	$\alpha_{ox}$ (9)	Comment (10)
000202.5–103030 .....	000202.95–103038.0	17.42	0.103	14.25	43.61	28.87	25.07	1.46	Sy 1.8, radio
000250.8+000824 .....	000251.60+000800.7	19.35	0.107	10.03	43.49	28.13	24.96	1.22	Sy 1.5
001056.7–090100 .....	001056.25–090109.9	17.92	0.081	6.87	43.07	28.45	24.53	1.50	Sy 1.8
001618.5+011528 .....	001617.83+011522.0	19.56	0.217	8.89	44.13	28.70	25.60	1.19	Sy 1.8
002608.2–000544 .....	002608.38–000547.0	19.48	0.107	4.87	43.18	28.08	24.64	1.32	Sy 2?, radio

NOTES.—Table 4 is published in its entirety in the electronic edition of the *Astronomical Journal*. A portion is shown here for guidance regarding its form and content.

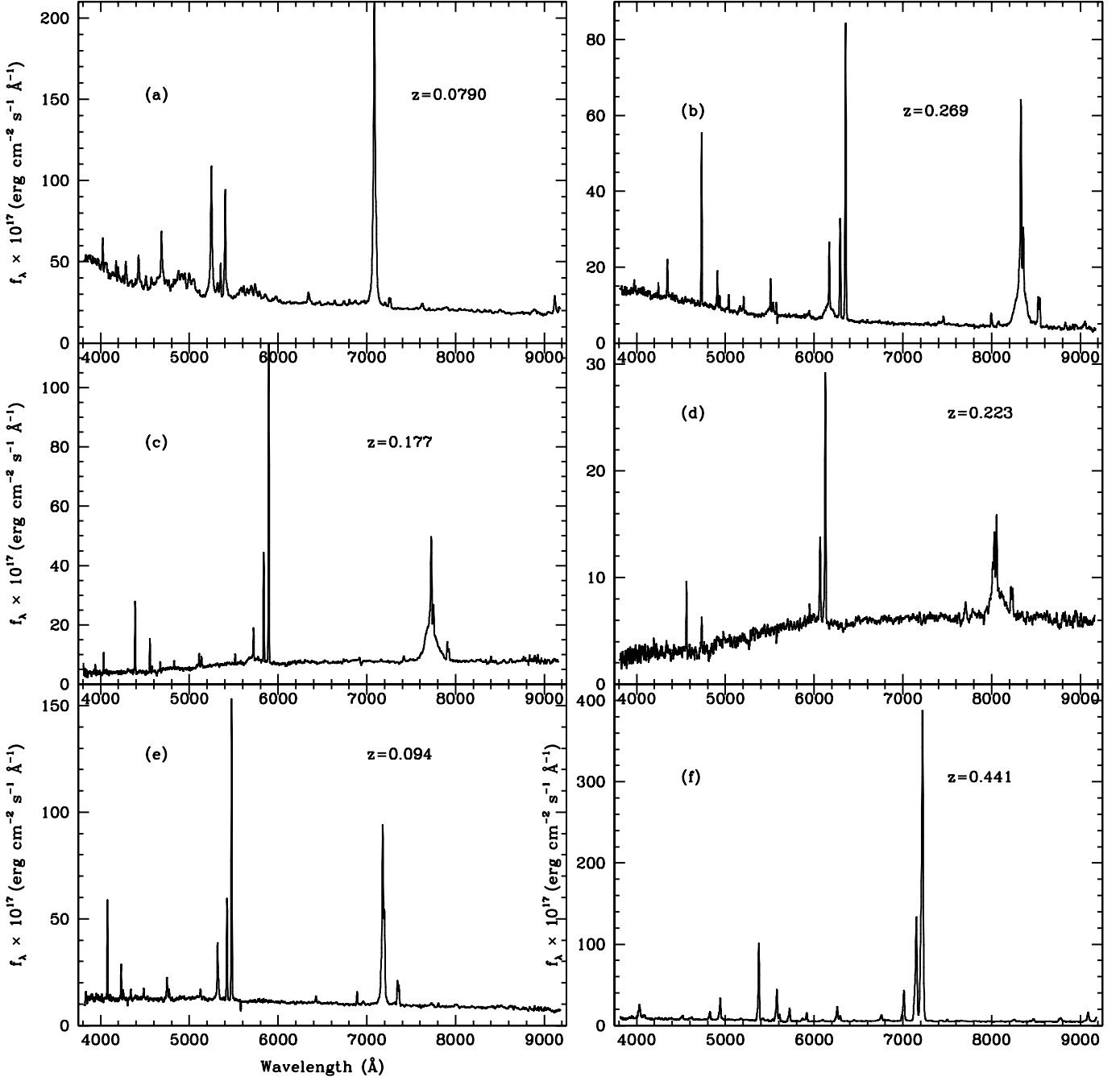


FIG. 3.—Selected SDSS optical spectra for RASS/SDSS X-ray-emitting quasars/AGNs with narrower permitted emission components, chosen to reflect the diversity among the 515 objects cataloged in § 3.2. Approximate spectral taxonomical classifications for (a–f) are NLS1, Seyfert 1.5, Seyfert 1.8, Seyfert 1.9, Seyfert 2, and a possible type 2 quasar, respectively (see Zakamska et al. [2003] for a discussion of SDSS type 2 quasars). (a) SDSS J141755.54+431155.8. (b) SDSS J142337.63+341052.9. (c) SDSS J155021.40+295027.8. (d) SDSS J085348.18+065447.1. (e) SDSS J143001.63+455049.1. (f) SDSS J091345.48+405628.2.



TABLE 5  
OBSERVED PARAMETERS OF RASS/SDSS BL LAC CANDIDATES

RASS X-Ray Source RXS J (1)	SDSS Optical Counterpart SDSS J (2)	<i>u</i> (3)	<i>g</i> (24)	<i>r</i> (5)	<i>i</i> (6)	<i>z</i> (7)	Opt. Morphology (8)	Redshift (9)	X-Ray Count Rate (10)	Exp. Time (11)	HR1 (12)	HR2 (13)	Det. Likelihood (14)	$f_X \times 10^{13}$ (15)
002200.9+000659 .....	002200.95+000657.9	20.48	20.03	19.28	18.87	18.55	3	0.306	0.0973	403	0.08	0.12	55	9.05
003514.9+151513 .....	003514.72+151504.1	17.32	16.93	16.59	16.31	16.05	6	1.090	0.2358	359	0.35	0.25	235	26.95
005041.0−092855 .....	005041.31−092905.1	16.78	16.30	16.03	15.77	15.57	6	...	0.1974	536	0.06	0.16	256	21.34
005620.1−093626 .....	005620.07−093629.8	18.33	17.55	16.96	16.66	16.30	3	0.103	0.3558	335	0.52	0.14	298	38.70
014126.8−092857 .....	014125.83−092843.6	18.11	17.59	17.21	16.97	16.68	6	0.500	0.0344	440	−0.01	0.24	25	3.20

NOTES.—Table 5 is published in its entirety in the electronic edition of the *Astronomical Journal*. A portion is shown here for guidance regarding its form and content.

TABLE 6  
DERIVED PARAMETERS OF RASS/SDSS BL Lac CANDIDATES

RASS X-Ray Source RXS J (1)	SDSS Optical Counterpart SDSS J (2)	$g_o$ (3)	Redshift (4)	$f_X^c \times 10^{13}$ (5)	$\log(L_X)$ (6)	$\log(l_{\text{opt}})$ 2500 Å (7)	$\log(l_X)$ 2 keV (8)	$\alpha_{\text{ox}}$ (9)	Comment (10)
002200.9+000659 .....	002200.95+000657.9	19.94	0.306	21.02	44.86	28.87	26.33	0.98	BL?, radio
003514.9+151513 .....	003514.72+151504.1	16.67	1.090	73.75	46.84	31.41	28.30	1.19	zunc, radio
005041.0–092855 .....	005041.31–092905.1	16.18	...	55.50	...	...	...	1.39	zunc, radio, FBQSJ0050–0929
005620.1–093626 .....	005620.07–093629.8	17.37	0.103	101.2	44.46	28.89	25.92	1.14	BL?, radio,
014126.8–092857 .....	014125.83–092843.6	17.48	0.500	7.42	44.94	30.33	26.41	1.50	zunc, radio, [HB89]0138–097

NOTES.—Table 6 is published in its entirety in the electronic edition of the *Astronomical Journal*. A portion is shown here for guidance regarding its form and content.

85 additional objects that are within RASS error circles and that either satisfy the first three criteria (X-ray/radio sources with no strong optical emission) but have slightly larger Ca II H and K breaks with  $0.25 < C < 0.4$  (see Marchã et al. 1996); have too low S/N in their SDSS optical spectra to claim with confidence the BL Lac spectral nature of criteria 3 and 4; or show approximately featureless SDSS spectra, i.e., satisfy criteria 1, 3, and 4 but there is no close match to a radio source. The latter seven objects are of potentially high interest for additional follow-up as unusually weak radio sources; the vast majority of confidently identified BL Lac objects cataloged thus far are radio sources (although some are weak).

The 5740 deg<sup>2</sup> of sky considered here thereby includes a total of 266 candidate X-ray BL Lac counterparts, and basic information for them is provided in Tables 5 and 6. An entry of “zunc” in the comment column of Table 6 denotes cases for which a redshift from SDSS or the literature is unavailable or highly uncertain. If a redshift is not obtained from the SDSS spectrum nor available in the literature, we adopt  $z = 0.3$  (near the median of others in the sample) for estimating  $\alpha_{\text{ox}}$  in Table 6; as this is essentially a distance-independent ratio of luminosities, the values of  $\alpha_{\text{ox}}$  should be approximately correct in most cases, except for precise values of spectral  $K$ -corrections. In Table 6 we denote the possible but less certain BL Lac candidates as “BL?” in the comment column. Example SDSS spectra of representative X-ray BL Lac candidates are shown in Figure 4.

About half of these objects were first identified as BL Lac candidates via SDSS and/or have redshifts first reliably measured from SDSS spectroscopy (although some, e.g., are cataloged in Bade et al. [1998b] but lacked secure identifications and/or redshifts in their low-resolution prism data). About 40% of the full sample of 266 currently have reasonably confident SDSS or published spectroscopic redshifts, and another 20% have less confident spectroscopic redshift estimates.

As an added precaution to limit contamination of the BL Lac sample by stars with weak features (e.g., DC white dwarfs), we have also considered proper-motion information, as in Collinge et al. (2005). We obtained proper motions from the SDSS database for 242 of our 266 RASS/SDSS BL Lac candidates. Of these 242, only 4 BL Lac candidates appear to have significant proper motion ( $>20$  mas yr<sup>−1</sup>). However, three of the latter candidates have secure extragalactic redshifts from their SDSS spectra, and the fourth object is cataloged as a confirmed BL Lac object by Veron-Cetty and Veron.<sup>10</sup> All four candidates additionally match to both an X-ray and a radio source, suggesting little contamination by nearby hot white dwarfs. Thus, it seems

likely that most of the BL Lac identifications are correct (see also § 5 below).

This catalog of RASS/SDSS/radio-selected BL Lac candidates constitutes one of the largest samples obtained to date (see also Collinge et al. [2005] for a similarly large optically selected sample from SDSS). Each is accompanied by uniform X-ray, optical, and radio data.

#### 4. OTHER RARE CLASSES OF X-RAY-EMITTING AGNs

##### 4.1. Narrow-Line Seyfert 1 Galaxies

In our expanded DR5 RASS/SDSS sample we identify from SDSS spectra a total of 774 candidate X-ray-emitting NLS1s. These include objects cataloged in both §§ 3.1 and 3.2, and they are denoted by “NLS1?” in the comment columns of Tables 2 and 4. Williams et al. (2002) discussed 45 of these SDSS X-ray NLS1s independently selected from the SDSS Early Data Release, and we added 120 more in Paper I. In the optical, NLS1s have unusually narrow permitted lines, although in most other ways they resemble Seyfert 1 more than Seyfert 2 galaxies; in the X-ray they often show strong soft X-ray excesses and marked variability. Various explanations have been suggested for NLS1s; e.g., unusually low mass black holes and/or higher accretion rates relative to Eddington (see reviews by Boller 2000; Pogge 2000).

The 774 X-ray-emitting candidate NLS1s all have the following spectral characteristics, representative of the NLS1 class (e.g., Pogge 2000): [O III]  $\lambda$ 5007-to- $H\beta$  flux ratios of less than 1 (from the SDSS spectroscopic pipeline Gaussian-fit emission-line measures),  $H\beta$  FWHM (again from the SDSS spectroscopic pipeline) less than 2000 km s<sup>−1</sup>, and strong optical Fe emission. Seventy-four of these are detected in the FIRST radio survey; these are of possible special interest, as radio-loud NLS1s may be unusually rare (e.g., Komossa et al. 2006). An example SDSS spectrum for a NLS1 candidate is shown in Figure 3a.

##### 4.2. BALQSOs

ROSAT studies extending back more than a decade (Green et al. 1995), along with many subsequent investigations, demonstrated that BALQSOs as a class are weak emitters in soft X-rays. The soft X-ray deficiency is thought to arise due to absorption in BAL material of high column density, typically inferred as equivalent to  $N_H \sim 10^{22}$ – $10^{23}$  cm<sup>−2</sup> (e.g., Green et al. 2001; Gallagher et al. 2002). In our DR5 sample there are 14 cases of traditional BALQSOs (i.e., those with “balnicity index” BI > 0) that fall within 1′ RASS error circles, plus another two dozen cases with weaker BALs and/or possible mini-BALs. (See Trump et al. [2006] for an extensive recent discussion and catalog of SDSS BALQSOs, selected based on both the standard

<sup>10</sup> VizieR Online Data Catalog, 7248 (M. P. Veron-Cetty & P. Veron, 2006).

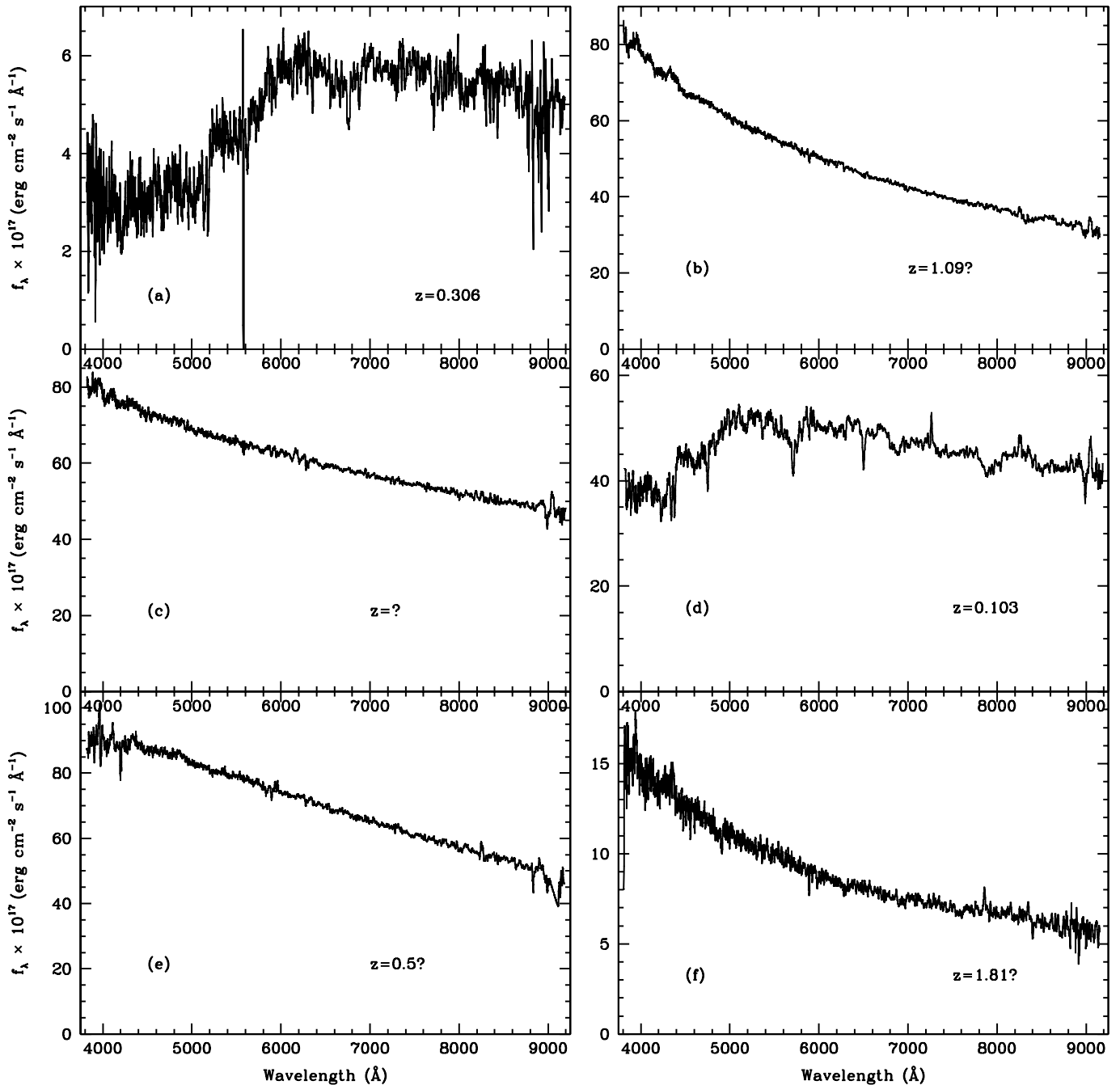


FIG. 4.—Representative SDSS optical spectra for RASS/SDSS X-ray-emitting BL Lac candidates as discussed in § 3.3. Shown (a–e) are spectra for the first five objects listed in Tables 5 and 6, along with (f) a possible high-redshift case. A total of 266 such BL Lac candidates are presented in our updated RASS/SDSS catalog. (a) SDSS J002200.95+000657.9. (b) SDSS J003514.72+151504.1. (c) SDSS J005041.31–092905.1. (d) SDSS J005620.07–093629.8. (e) SDSS J014125.83–092843.6. (f) SDSS J124700.72+442318.7.

Weymann et al. [1991] BI criteria as well as the more inclusive absorption-line index or AI criteria of Hall et al. [2002]). Of course, in some cases an improved X-ray position may be required to definitively establish whether all these BALQSOs are actually the X-ray-source counterparts, given the expected (see § 5) few percent contamination of our full AGN sample. Shown in Figure 5a is the SDSS spectrum of an example X-ray-emitting BALQSO.

Although definitive conclusions await further confirmations of which BALQSOs are genuine X-ray sources and which are just chance coincidences, the RASS/SDSS sample size is now large enough to begin to provide some ensemble statistical tests

of the (anticipated low) incidence of X-ray-emitting BALQSOs. For example, the Trump et al. (2006) SDSS study found an incidence of 10.4% (with a formal statistical error of about 0.2%) for mainly optically selected  $BI > 0$  BALQSOs among DR3 quasars with  $z > 1.7$ . The analogous BALQSO incidence in our RASS/SDSS X-ray-selected sample is  $4.6\% \pm 1.5\%$ , i.e., a significantly smaller incidence in a soft X-ray-selected sample (at least) at the  $>3\sigma$  level. In the latter estimate we consider just the DR3 subset for maximum consistency with the Trump et al. study; this is really an upper limit on the incidence in the RASS/SDSS sample, as it somewhat optimistically assumes that all  $BI > 0$  cases are genuine X-ray/BALQSO associations.

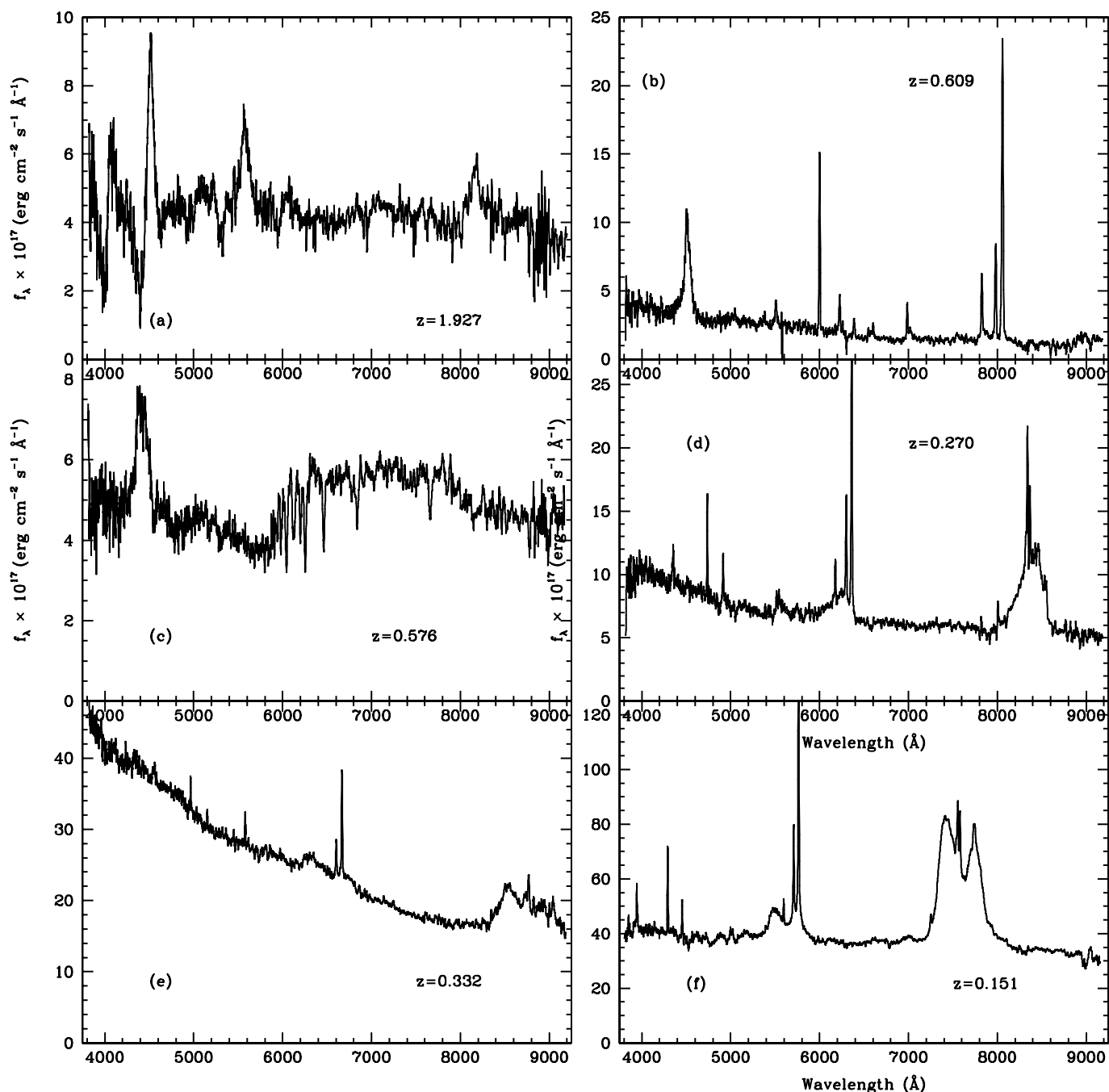


FIG. 5.—Selected other RASS/SDSS X-ray-emitting AGNs having unusual optical SDSS spectral characters. (a) SDSS J105626.95+482956.3 is an example of a possible X-ray-emitting BALQSO. (b) SDSS J074951.42+204936.9 is an AGN with a weak, narrow  $H\beta$  line characteristic of a Seyfert 1.8–2 galaxy but a strong, broad  $Mg\ II$  line. (c) SDSS J163446.49+461946.7 is a poststarburst AGN. (d) SDSS J115227.12+604817.4 and (e) SDSS J102738.53+605016.5 are examples of AGNs with broad, asymmetric Balmer profiles. (f) SDSS J161742.53+322234.3 is an example X-ray-emitting AGN with unusual multiple-peaked and broad emission line profiles (SDSS J1027+6050 may also be double-peaked).

#### 4.3. Unusual Line Profiles and Other Odd Cases

There are many further quasars in our updated catalog with unusual optical line profiles (see Paper I for further discussion). These include further examples of X-ray-emitting AGNs with weak/narrow  $H\beta$  characteristic of Seyfert 1.8–2 galaxies but also having strong broad  $Mg\ II$  (Fig. 5b), poststarburst AGNs (Fig. 5c), AGNs with broad asymmetric Balmer profiles (Figs. 5d and 5e), and X-ray AGNs with highly unusual multiple-peaked emission-line profiles (Figs. 5e and 5f).

#### 5. ENSEMBLE PROPERTIES AND IDENTIFICATION RELIABILITY

From the expanded  $5740\ \text{deg}^2$  of sky coverage in DR5 7000 quasars or other AGNs are identified as likely RASS counterparts, each with uniform and high-quality optical photometry and spectroscopy from SDSS and X-ray data from *ROSAT*. The ensemble X-ray flux, optical magnitude, and redshift distributions are depicted in Figure 6. The X-ray flux distribution (Fig. 6a) reflects the typical depth of the RASS catalogs, with

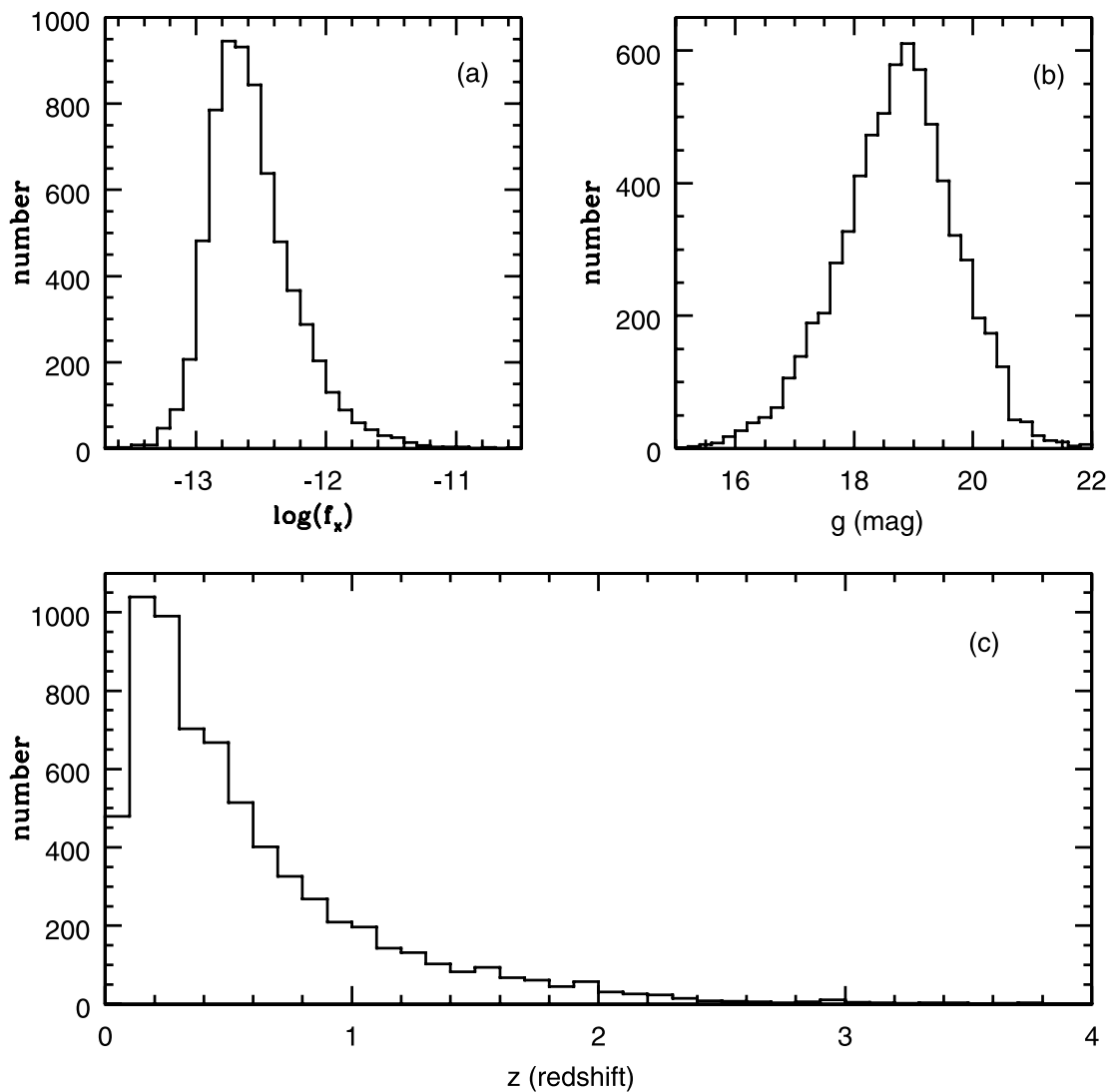


FIG. 6.—Distributions of (a) RASS X-ray fluxes, (b) SDSS  $g$ -band magnitudes, and (c) redshifts for 6700 AGN counterparts of RASS/SDSS X-ray-emitting AGNs. (BL Lac objects are excluded from the plots here, as many have uncertain redshifts.) The median magnitude ( $g = 18.8$ ) and redshift ( $z = 0.42$ ) are typical of other optical identification efforts at comparable X-ray depth (median  $f_X = 2.5 \times 10^{-13}$  ergs s $^{-1}$  cm $^{-2}$ ), although the very large sample includes a substantial number of bright or higher redshift AGNs as well.

median  $f_X = 2.5 \times 10^{-13}$  ergs s $^{-1}$  cm $^{-2}$ ; the optical magnitude (Fig. 6b) and redshift (Fig. 6c) distributions of the AGNs remain typical of past identification work at comparable X-ray depth, with medians  $g = 18.8$  and  $z = 0.42$ . However, our updated RASS/SDSS catalog is sufficiently large to, for example, include 162  $z > 2$  X-ray-emitting AGNs, 334 having  $g < 17$  and 505 with  $f_X > 10^{-12}$  ergs s $^{-1}$  cm $^{-2}$ . Note that in our sample, which is affected by both X-ray and optical flux limits, luminosities and redshift are strongly coupled (Fig. 7).

In our expanded DR5 catalog, the distributions of offsets between RASS X-ray positions and SDSS optical positions are again approximately as expected if most of the 7000 AGNs are the proper identifications. For example, 86% of the SDSS quasars/AGNs fall within 30'' of the RASS X-ray positions (see the angular offset distribution in Fig. 8a), in approximate agreement with the RASS positional uncertainty distribution, independently derivable from Tycho stars also detected in RASS (Voges et al. 1999). In Figure 8b these angular offsets have been normalized relative to their associated estimated RASS positional errors to better account for the dependence of the RASS positional uncertainty on the X-ray-source significance, etc. This

figure confirms that the RASS positional error estimates are reasonable, with 98% of the suggested identifications at offsets smaller than  $3\sigma$  (where  $\sigma$  is the estimated RASS X-ray positional error); we also note, however, that the distribution of RASS positional errors may not be fully characterized by either a simple one- or two-dimensional Gaussian (Agüeros et al. 2006). Figure 9 shows the distributions of the squares  $r^2$  of the offsets between the SDSS optical positions and the RASS X-ray-source positions for various AGN subclasses considered herein; specifically, we display the fraction of suggested SDSS counterparts falling within equal area annuli offset from the RASS X-ray-source positions. For a chance superposition of SDSS objects within RASS error circles, these histograms would be approximately flat with  $r^2$ . But the respective distributions for broad-line AGNs (from § 3.1), narrow-line AGNs (§ 3.2), BL Lac objects (§ 3.3), and NLS1s (§ 4.1) are each strongly peaked at small  $r^2$  values, as expected if these AGNs are statistically the proper X-ray-source identifications.

Further quantifying the statistical reliability of these identifications is the following. The surface density of SDSS optically selected quasars is a little more than 12 deg $^{-2}$  (e.g., Schneider

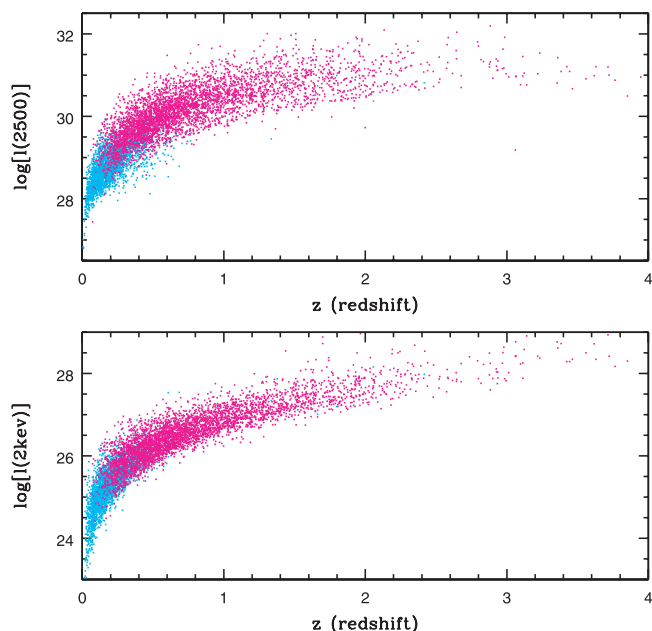


FIG. 7.—Luminosity and redshift are strongly coupled in our sample with both X-ray and optical limits (cgs monochromatic luminosities at frequencies corresponding to 2500 Å and 2 keV are shown). The magenta dots display data for quasi-stellar X-ray identifications that are unresolved in SDSS optical images, while cyan dots show data for AGNs that are morphologically resolved in SDSS.

et al. 2005), while the combined area covered by all RASS error circles considered in the 5740 deg<sup>2</sup> area of this updated sample is a little over 13 deg<sup>2</sup>. Thus, based on surface density arguments, only a small fraction (of order 3%) of the proposed quasar/AGN X-ray-source counterparts are likely to be spurious random chance positional coincidences. Similarly, if we randomly alter the positions in the RASS catalog by several arcminutes and then cross-correlate again between SDSS quasars and such synthetically offset RASS catalogs, we alternately estimate that only of order 5% of the SDSS AGNs cataloged herein are likely to be chance positional coincidences, unrelated to RASS X-ray sources.

The ratios  $f_X/f_{\text{opt}}$  of X-ray-to-optical flux for the identifications are also as expected for typical X-ray-emitting AGNs. Roughly as much energy is emitted in the X-ray as in the optical bands for typical quasars, as is reaffirmed by the empirical  $f_X/f_{\text{opt}}$  distribution shown in Figure 10a for the 6224 quasars/AGNs with predominant broad emission line regions considered in § 3.1. In estimating  $f_X/f_{\text{opt}}$  we here adopt the (corrected) 0.1–2.4 keV X-ray flux (e.g., from Table 2) and estimate the optical broadband flux in a 4000–9000 Å bandpass using the *g*-band PSF magnitudes (e.g., again from Table 2) assuming an optical power law in energy with index  $\alpha_o = 0.5$ . The observed  $f_X/f_{\text{opt}}$  distribution in Figure 10a for DR5 broad-line RASS/SDSS AGNs appears very similar to that found for EMSS quasars (see Stocke et al. 1991); two-sided Kolmogorov-Smirnov (K-S) comparisons between the EMSS and RASS/SDSS  $f_X/f_{\text{opt}}$  distributions for quasars confirm similarity at the 23%–61% level for a plausible range of conversions between the differing EMSS versus RASS/SDSS X-ray and optical passbands (and implicit spectral assumptions). Figure 10b shows the analogous distribution of  $f_X/f_{\text{opt}}$  ratios for the 266 RASS/SDSS BL Lac candidates discussed in § 3.3. This distribution also appears very similar to that found in earlier X-ray-selected BL Lac

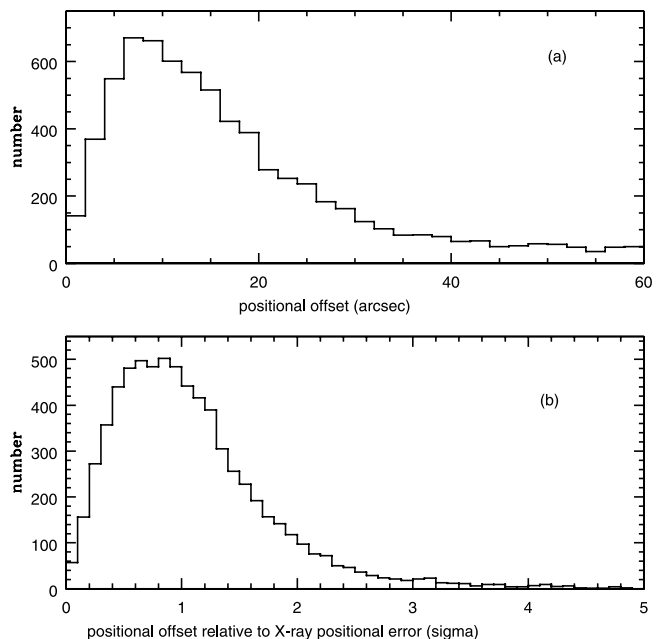


FIG. 8.—Distribution of differences between the SDSS optical and RASS X-ray positions of the 7000 AGNs cataloged here, which are consistent with expectations if most have the proper identifications. (a) Positional offset distribution in arcseconds, approximately as expected for the RASS positional accuracy. (b) Distribution of the differences between the SDSS optical and RASS X-ray positions, here normalized by their associated RASS X-ray-source positional errors (a handful of objects with relative offsets  $>5\sigma$  are excluded from this plot).

samples (e.g., again see Stocke et al. 1991); two-sided K-S tests indicate a match of EMSS and RASS/SDSS  $f_X/f_{\text{opt}}$  distributions for BL Lac objects at the 21%–64% level, with the range again reflecting uncertainties in conversions between systematically different passbands, etc. The broad agreement of the  $f_X/f_{\text{opt}}$  distributions with previous work for both quasars and BL Lac objects further confirms that the vast majority of the suggested RASS/SDSS identifications are likely correct.

## 6. AN EXAMPLE X-RAY/OPTICAL CORRELATION FROM THE EXPANDED SAMPLE

This paper primarily presents updated catalog information, but we also include below a brief update on our Paper I example of an X-ray/optical correlation. More generally, the large RASS/SDSS sample size and associated uniformity of X-ray and optical (and radio) data may be useful for other more detailed, multi-wave band follow-up studies (e.g., see Körding et al. 2006).

The 6224 X-ray-emitting AGNs with predominant broad-line regions discussed in § 3.1 show (see Fig. 11) the well-known correlation between (the logarithms of) optical and X-ray monochromatic luminosities found in many earlier studies/samples (e.g., Avni & Tananbaum 1986). We again caution (see Paper I) that our sample is, of course, an X-ray-selected sample with inherent X-ray biases. Nonetheless, the best-fit linear relationship we find (Fig. 11a) between the logarithms of X-ray and optical luminosities, equivalent to  $L_X \propto L_{\text{opt}}^{0.90 \pm 0.01}$ , is in good agreement with that found in other studies (e.g., see Wilkes et al. 1994; Green et al. 1995; Vignali et al. 2003; Paper I). This best-fit linear relation is virtually unchanged when excluding the 15% of the objects that are radio-detected.

As we suggested previously in Paper I, however, the best-fit slopes of the relation within our RASS/SDSS sample differ

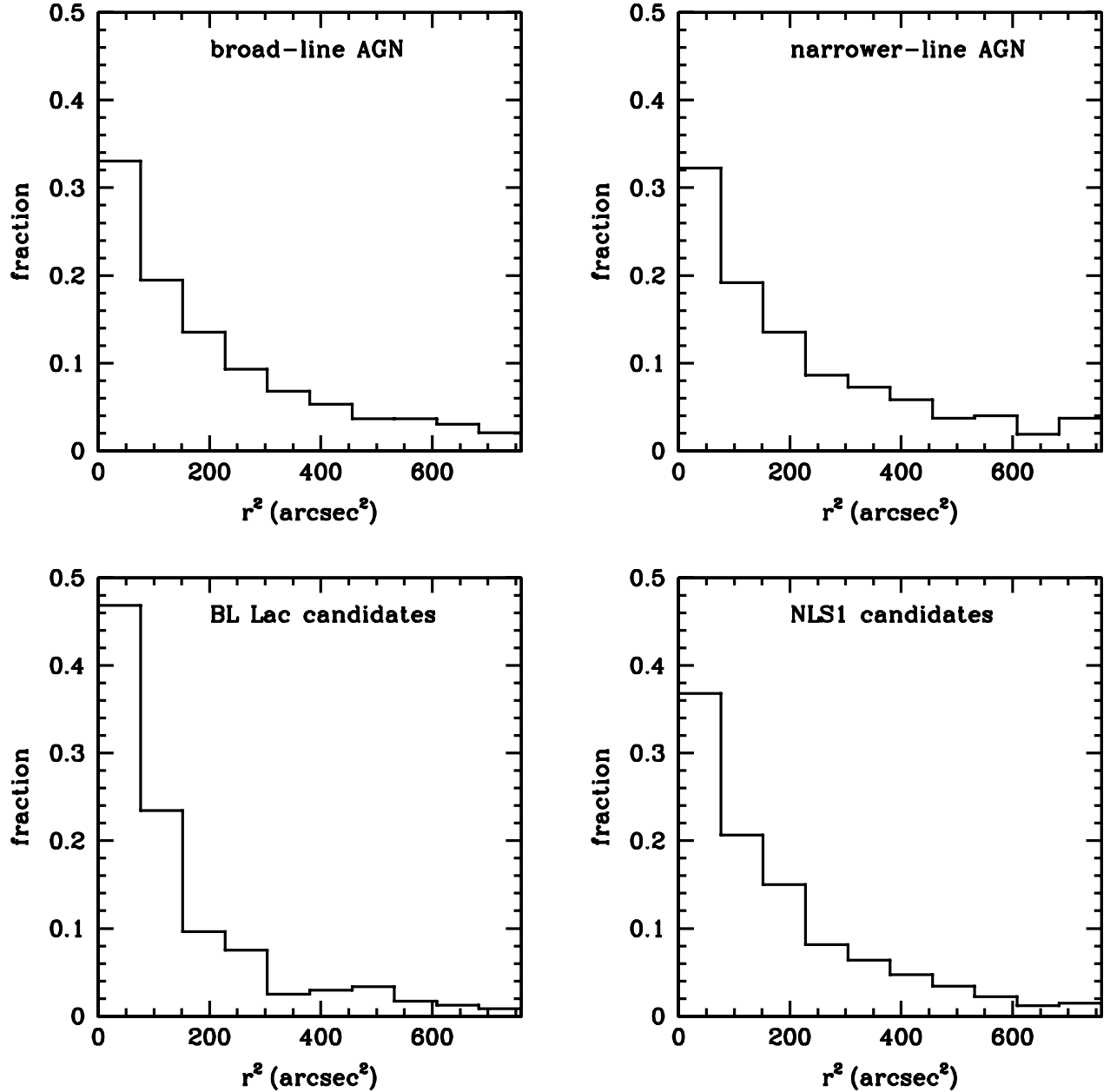


FIG. 9.—Distributions of the squares  $r^2$  of the offsets between the SDSS optical positions and the RASS X-ray-source positions; specifically, we display the fraction of optical counterparts falling within equal-area annuli offset from the RASS X-ray-source positions (we consider only objects within  $r < 27.5''$ , where all relevant algorithms for SDSS spectroscopy may select targets). Distributions are shown for quasars/AGNs with predominant broad lines discussed in § 3.1 (*top left*), quasars/AGNs with narrower permitted lines discussed in § 3.2 (*top right*), BL Lac candidates discussed in § 3.3 (*bottom left*), and candidate NLS1s discussed in § 4.1 (*bottom right*). In each case the distributions are very strongly peaked at small  $r^2$  values, as expected if these AGNs are statistically the proper X-ray-source identifications.

when separately considering lower versus higher optical luminosity objects. For example, if we divide the 6224 broad-line AGNs (§ 3.1) into two subsamples at the median value  $\log(l_{\text{opt}}) = 29.76$  (cgs) we find  $l_X \propto l_{\text{opt}}^{0.96 \pm 0.01}$  for the half below the median but  $l_X \propto l_{\text{opt}}^{0.85 \pm 0.02}$  for the half above the median optical luminosity; both these slope values are consistent with those we quoted in Paper I—although from a much smaller sample in that earlier paper—for a very similar luminosity division. If one restricts consideration to just the 406 objects in our DR5 sample with highest optical luminosity  $\log(l_{\text{opt}}) > 31$ , the best-fit slope of the logarithmic relation decreases even further, corresponding to  $l_X \propto l_{\text{opt}}^{0.50 \pm 0.09}$ . Very recently, some large studies (Steffen et al. 2006) based on optically selected samples have also begun to confirm that the best-fit slope in the relationship

between  $\log(l_X)$  and  $\log(l_{\text{opt}})$  may not be a constant but instead may itself depend on optical luminosity. Such a “nonlinear” relationship between  $\log(l_X)$  and  $\log(l_{\text{opt}})$  was suggested in our Paper I and earlier studies such as those of Yuan et al. (1998a). Such complicated possible dependences caution that when considering results among different studies it is useful to compare X-ray versus optical correlations for objects of similar luminosity.

One might alternately divide the sample between morphologically resolved AGNs and those that have optical stellar PSF morphology in SDSS images (see the type parameter in Table 1). With this subdivision one finds a similar result:  $l_X \propto l_{\text{opt}}^{0.97 \pm 0.02}$  for resolved AGNs compared with  $l_X \propto l_{\text{opt}}^{0.84 \pm 0.01}$  for stellar-morphology AGNs. Not too surprisingly, however, the resolved

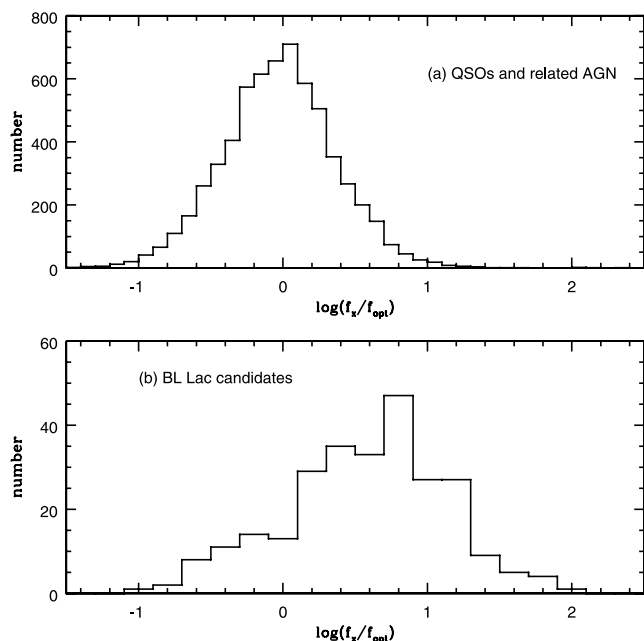


FIG. 10.—(a) Distribution of  $f_X/f_{\text{opt}}$  for the 6224 quasar/AGN identifications having predominant broad emission line regions (see § 3.1). The RASS/SDSS quasars/AGNs emit approximately as much energy in the X-ray as in the optical band, as expected if these are the proper identifications. (b) Distribution of  $f_X/f_{\text{opt}}$  for the RASS/SDSS BL Lac candidates discussed in § 3.3. The distribution is similar to that found in other X-ray-selected BL Lac surveys, affirming that these RASS/SDSS objects are also likely to be the proper identifications.

AGNs (for which optical host galaxy photometric contributions may be most problematic) are at systematically lower optical luminosity and redshift than the optically unresolved subset (Fig. 7). Further studies will be required to disentangle such strongly coupled parameters.

Regressing  $\alpha_{\text{ox}}$  against optical luminosity yields similar results. For the 6224 quasars/AGNs with observed broad-line regions discussed in § 3.1, this regression yields  $\alpha_{\text{ox}} \propto l_{\text{opt}}^{0.037 \pm 0.002}$ , approximately equivalent as expected to  $l_X \propto l_{\text{opt}}^{0.90}$ . Figure 11b depicts the relationship from the  $\alpha_{\text{ox}}$  perspective. The solid line shows the above linear best-fit regression relation with slope 0.037, while the error bars show the mean and the standard error in the mean value of  $\alpha_{\text{ox}}$ , as well as the mean and standard deviations of the optical luminosity, when considering averages taken in various logarithmic optical luminosity bins. (The vertical error bars account for the large number of data points averaged to estimate  $\langle \alpha_{\text{ox}} \rangle$  in each bin: typically 100–500, with a range of 42–534.) The offset of multiple independent and adjacent error bars significantly away from the simple best-fit line in Figure 11b further suggests the possibility of a more complicated relation than assumed in the standard linear regression of  $\alpha_{\text{ox}}$  versus  $\log(l_{\text{opt}})$ , or in the equivalent  $\log(l_X)$  versus  $\log(l_{\text{opt}})$  relation discussed above.

However, we reiterate our caution of Paper I that the multiple strongly correlated parameters involved here require a much more careful analysis, including proper accounting for and disentangling of the various selection biases, intertwined dependences on redshift and optical luminosity, disparate dispersions in optical compared with X-ray luminosities (e.g., Yuan et al. 1998b), host-galaxy photometric contamination, radio dependences, and so on. To highlight such complications we note that two recent studies on optically selected SDSS quasars having *ROSAT* information available arrive at rather different conclusions about whether  $\alpha_{\text{ox}}$  may also depend on redshift as well as

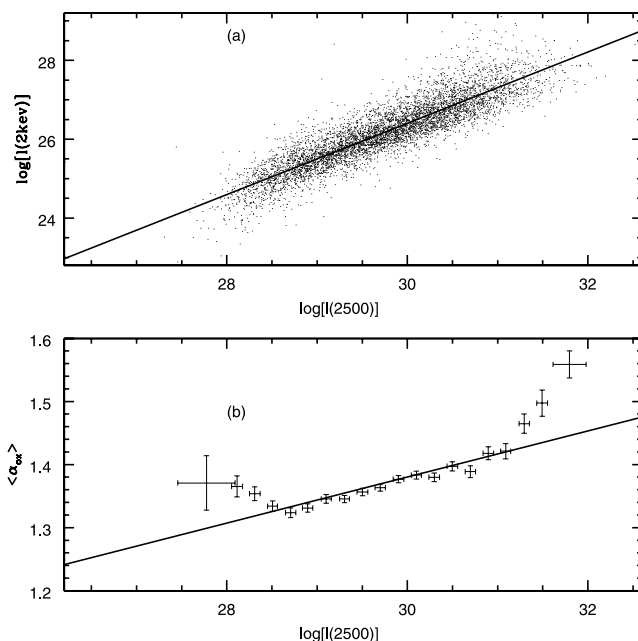


FIG. 11.—X-ray-selected sample of 6224 quasars/AGNs with predominant broad emission line regions, showing the well-known relationship between X-ray and optical wave bands (logarithms of monochromatic luminosities in cgs units at 2 keV and 2500 Å are used). (a) The solid line is a linear least-squares fit to the logarithms of  $l_{2\text{keV}}$  vs.  $l_{2500}$  data, with slope  $0.90 \pm 0.01$ . (b) Consistent results are obtained when regressing  $\alpha_{\text{ox}}$  against optical luminosity, and in this case a simple linear regression yields  $\alpha_{\text{ox}} \propto l_{\text{opt}}^{0.037}$ , equivalent, as expected, to  $l_X \propto l_{\text{opt}}^{0.90}$ . The solid line is the best-fit linear regression relation when fitted to all 6224 points separately; the error bars show the mean and the standard error in the mean value of  $\langle \alpha_{\text{ox}} \rangle$ , as well as the mean and standard deviations in optical luminosity, when considering averages taken in various logarithmic optical luminosity bins (typically with 100–500 points per bin). The deviation of multiple adjacent, and independent, error bars significantly away from the simple best-fit line suggests the possibility of a more complicated relation than is assumed in standard linear regression models.

optical luminosity (Shen et al. 2006; Steffen et al. 2006). As noted above, these two parameters (and others) are certainly strongly correlated in our RASS/SDSS sample, with flux limits in both the X-ray and the optical (Fig. 7).

## 7. SUMMARY

The SDSS optical and RASS X-ray surveys are well matched to each other, allowing efficient large-scale identification of X-ray-source optical counterparts. Application of our approach to SDSS DR5 data has provided homogeneous identification and RASS/SDSS flux and spectroscopic data for a large sample of X-ray-emitting quasars and other kinds of AGNs. The combination of SDSS multicolor selection and RASS data—and, in some cases, FIRST radio information—is highly efficient for the selection of X-ray-emitting quasars/AGNs. In our updated analysis encompassing 5740 deg<sup>2</sup> of sky, 7000 plausible X-ray-emitting quasars/AGNs have been optically identified, including hundreds of rare cases such as BL Lac objects and NLS1s. The RASS/SDSS survey is rapidly approaching  $\sim 10^4$  fully and homogeneously characterized optical counterpart identifications. The large sample will allow for a variety of more detailed studies of various AGN subclasses and individual objects of special interest, as well as studies of ensemble correlations between optical and X-ray wave bands. In closing, we also note that many of the cataloged objects have X-ray fluxes accessible to at least the next generation of envisioned high-quality X-ray spectroscopy experiments, such as *Constellation-X*.



S. F. Anderson and R. M. Plotkin gratefully acknowledge support from NASA/ADP grant NNG 05GC45G. We thank Jonathon Trump for useful discussions. Funding for the SDSS and SDSS-II has been provided by the Alfred P. Sloan Foundation, the Participating Institutions, the National Science Foundation, the US Department of Energy, the National Aeronautics and Space Administration, the Japanese Monbukagakusho, the Max Planck Society, and the Higher Education Funding Council for England. The SDSS Web site is at <http://www.sdss.org>. The SDSS is managed by the Astrophysical Research Consortium for the Participating Institutions. The Participating Institutions are the American Museum of Natural History, Astrophysical Insti-

tute Potsdam, the University of Basel, Cambridge University, Case Western Reserve University, the University of Chicago, Drexel University, Fermilab, the Institute for Advanced Study, the Japan Participation Group, Johns Hopkins University, the Joint Institute for Nuclear Astrophysics, the Kavli Institute for Particle Astrophysics and Cosmology, the Korean Scientist Group, the Chinese Academy of Sciences, Los Alamos National Laboratory, the Max Planck Institute for Astronomy, the Max Planck Institute for Astrophysics, New Mexico State University, Ohio State University, the University of Pittsburgh, the University of Portsmouth, Princeton University, the US Naval Observatory, and the University of Washington.

## REFERENCES

- Adelman-McCarthy, J., et al. 2006, *ApJS*, 162, 38  
 Agüeros, M. A., et al. 2006, *AJ*, 131, 1740  
 Anderson, S. F., et al. 2003, *AJ*, 126, 2209 (Paper I)  
 Avni, Y., & Tananbaum, H. 1986, *ApJ*, 305, 83  
 Bade, N., Beckmann, V., Douglas, N. G., Barthel, P. D., Engels, D., Cordis, L., Nass, P., & Voges, W. 1998b, *A&A*, 334, 459  
 Bade, N., et al. 1998a, *A&AS*, 127, 145  
 Baldwin, J. A., Phillips, M. M., & Terlevich, R. 1981, *PASP*, 93, 5  
 Becker, R. H., White, R. L., & Helfand, D. J. 1995, *ApJ*, 450, 559  
 Blanton, M. R., Lupton, R. H., Maley, F. M., Young, N., Zehavi, I., & Loveday, J. 2003, *AJ*, 125, 2276  
 Bolter, Th. 2000, *NewA Rev.*, 44, 387  
 Collinge, M. J., et al. 2005, *AJ*, 129, 2542  
 Condon, J. J., Cotton, W. D., Greisen, E. W., Yin, Q. F., Perley, R. A., Taylor, G. B., & Broderick, J. J. 1998, *AJ*, 115, 1693  
 Dressler, A., & Schectman, S. 1987, *AJ*, 94, 899  
 Flesch, E., & Hardcastle, M. J. 2004, *A&A*, 427, 387  
 Fukugita, M., Ichikawa, T., Gunn, J. E., Doi, M., Shimasaku, K., & Schneider, D. P. 1996, *AJ*, 111, 1748  
 Gallagher, S. C., Brandt, W. N., Chartas, G., & Garmire, G. P. 2002, *ApJ*, 567, 37  
 Gioia, I. M., Maccacaro, T., Schild, R. E., Stocke, J. T., Liebert, J. W., Danziger, I. J., Kunth, D., & Lub, J. 1984, *ApJ*, 283, 495  
 Green, P. J., Aldcroft, T. L., Mathur, S., Wilkes, B. J., & Elvis, M. 2001, *ApJ*, 558, 109  
 Green, P. J., et al. 1995, *ApJ*, 450, 51  
 Gunn, J. E., et al. 1998, *AJ*, 116, 3040  
 ———. 2006, *AJ*, 131, 2332  
 Hall, P. B., et al. 2002, *ApJS*, 141, 267  
 Halpern, J. P., Turner, T. J., & George, I. M. 1999, *MNRAS*, 307, L47  
 Hao, L., et al. 2005, *AJ*, 129, 1795  
 Hogg, D. W., Finkbeiner, D. P., Schlegel, D. J., & Gunn, J. E. 2001, *AJ*, 122, 2129  
 Ivezić, Z., et al. 2004, *Astron. Nachr.*, 325, 583  
 Kewley, L. J., Dopita, M. A., Sutherland, R. S., Heisler, C. A., & Trevena, J. 2001, *ApJ*, 556, 121  
 Komossa, S., Voges, W., Adorf, H.-A., Xu, D., Mathur, S., & Anderson, S. F. 2006, *ApJ*, 639, 710  
 Körding, E. G., Jester, S., & Fender, R. 2006, *MNRAS*, 372, 1366  
 Landt, H., Padovani, P., & Giommi, P. 2002, *MNRAS*, 336, 945  
 Laurent-Muehleisen, S. A., Kollgaard, R. I., Ryan, P. J., Feigelson, E. D., Brinkmann, W., & Siebert, J. 1997, *A&AS*, 122, 235  
 Lupton, R. H., Gunn, J. E., & Szalay, A. 1999, *AJ*, 118, 1406  
 Marchã, M. J. M., Browne, I. W. A., Impey, C. D., & Smith, P. S. 1996, *MNRAS*, 281, 425  
 Mickaelian, A. M., Hovhannisyan, L. R., Engels, D., Hagen, H.-J., & Voges, W. 2006, *A&A*, 449, 425  
 Morris, S. L., Stocke, J. T., Gioia, I., Schild, R. E., Wolter, A., Maccacaro, T., & della Ceca, R. 1991, *ApJ*, 380, 49  
 Perlman, E. S., et al. 1996, *ApJS*, 104, 251  
 Pfeiffermann, E., et al. 1987, *Proc. SPIE*, 733, 519  
 Pier, J. R., Munn, J. A., Hindsley, R. B., Hennessy, G. S., Kent, S. M., Lupton, R. H., & Ivezić, Z. 2003, *AJ*, 125, 1559  
 Pogge, R. W. 2000, *NewA Rev.*, 44, 381  
 Richards, G. T., et al. 2002, *AJ*, 123, 2945  
 Schartel, N., et al. 1996, *MNRAS*, 283, 1015  
 Schlegel, D. J., Finkbeiner, D. P., & Davis, M. 1998, *ApJ*, 500, 525  
 Schneider, D. P., et al. 2005, *AJ*, 130, 367  
 Shen, S., White, S. D. M., Mo, H. J., Voges, W., Kauffmann, C., & Anderson, S. F. 2006, *MNRAS*, 369, 1639  
 Smith, J. A., et al. 2002, *AJ*, 123, 2121  
 Stark, A. A., Gammie, C. F., Wilson, R. W., Bally, J., Linke, R. A., Heiles, C., & Hurwitz, M. 1992, *ApJS*, 79, 77  
 Steffen, A. T., Strateva, I., Brandt, W. N., Alexander, D. M., Koekemoer, A. M., Lehmer, B. D., Schneider, D. P., & Vignali, C. 2006, *AJ*, 131, 2826  
 Stocke, J. T., et al. 1991, *ApJS*, 76, 813  
 Stoughton, C., et al. 2002, *AJ*, 123, 485  
 Trump, J., et al. 2006, *ApJS*, 165, 1  
 Tucker, D., et al. 2006, *Astron. Nachr.*, 327, 821  
 Urry, C. M., & Padovani, P. 1995, *PASP*, 107, 803  
 Vanden Berk, D. E., et al. 2005, *AJ*, 129, 2047  
 Vignali, C., Brandt, W. N., & Schneider, D. P. 2003, *AJ*, 125, 433  
 Voges, W., et al. 1999, *A&A*, 349, 389  
 ———. 2000, *IAU Circ.* 6420  
 Weymann, R. J., Morris, S. L., Foltz, C. B., & Hewett, P. C. 1991, *ApJ*, 373, 23  
 Wilkes, B. J., Tananbaum, H., Worrall, D. M., Avni, Y., Oey, M. S., & Flanagan, J. 1994, *ApJS*, 92, 53  
 Williams, R. J., Pogge, R. W., & Mathur, S. 2002, *AJ*, 124, 3042  
 York, D. G., et al. 2000, *AJ*, 120, 1579  
 Yuan, W., Brinkmann, W., Siebert, J., & Voges, W. 1998a, *A&A*, 330, 108  
 Yuan, W., Siebert, J., & Brinkmann, W. 1998b, *A&A*, 334, 498  
 Zakamska, N. L., et al. 2003, *AJ*, 126, 2125  
 Zickgraf, F.-J., Engels, D., Hagen, H.-J., Reimers, D., & Voges, W. 2003, *A&A*, 406, 535